Economic Efficiency and Carbon Emissions in Multi-Energy Systems with Flexible Buildings

Zachary L. Hurwitz*, Yves Dubief*, and Mads Almassalkhi†
University of Vermont
College of Engineering and Mathematical Sciences
Burlington, Vermont, U.S.A.

Abstract

Multi-energy systems (MES) offer an opportunity to leverage energy conversion processes and temporary energy storage mechanisms to reduce costs and emissions during operation of buildings, campuses, and cities. With increasing options for flexibility in demand-side resources, it is possible to temporarily defer thermal and electrical demand of (flexible) buildings without sacrificing comfort and convenience of its occupants, which can improve overall MES economic efficiency and reduce emissions.

To that effect, this paper develops a linear optimization formulation of a MES with flexible (thermal and electric) building demands that capture nonlinearities in the efficiencies of energy conversion processes. The optimizaiton formulation accounts for multiple time-steps to capture the (first-order) dynamics of large thermal building loads. The flexible buildings are parameterized, in part, based on historical data from a college campus in Vermont, USA. The idea of the MES model is to investigate the role that flexible building loads plays in reducing costs and emissions for a small campus relative to that of a possible carbon tax. The operation of the MES is optimized to reduce costs based on representative seasons and carbon tax scenarios. Interestingly, it is found that when utilized optimally, flexible buildings can offer an effective method to improve economic efficiency while also reducing carbon emissions close to the levels that a carbon tax would realize, though without carbon price's large cost increases. That is, we present evidence that flexible buildings in Vermont may offer another route to achieve the emission goals close to that of a carbon tax policy.

Keywords

Multi-energy systems, buildings, flexibility, economic dispatch, carbon, optimization

*Z. Hurwitz and Y. Dubief are with the Department of Mechanical Engineering at the University of Vermont. Emails: {zhurwitz, ydubief}@uvm.edu

†M. Almassalkhi is with the Department of Electrical and Biomedical Engineering at the University of Vermont and was partly supported by the U.S. Department of Energy's Office of Energy Efficiency and Renewable Energy (EERE) award DE-EE0008006. Corresponding author: malmassa@uvm.edu.

1 Motivation & Introduction

Recently, climate change has intensified the focus on efficiency and methods to reduce carbon (and other harmful) emissions from human and engineering processes [1, 2]. This has led to innovations in building and renewable energy technologies and significantly tightened energy efficiency standards. In fact, it is well-recognized that the passive nature of efficiency alone is not sufficient to enable the deep penetration of variable renewable generation required to reverse the trends of climate change. Thus, to go beyond efficiency, we need to leverage the flexibility that is available behind the natural gas and electric meters, which could come from homes [3, 4], commercial buildings [5, 6, 7], and large industrial sites (i.e., commercial and industrial or C&I systems), such as manufacturing and campuses [8, 9, 10]. This has even motivated organizations, such as LEED, to recently update their energy efficiency certification metrics to explicitly include and incentivize demand-side flexibility [11].

The need for efficiency and flexibility should include multiple demand types, such as electric, (district) heating, and cooling. In fact, both natural gas and electricity often supply commercial and industrial (C&I) multi-energy systems (MES) and buildings from vast multi-energy carrier networks of pipelines and transmission lines that physically couple the electric, heating, and cooling demands. Therefore, to improve efficiency and leverage flexibility requires a multi-energy systems (MES) approach that is cognizant of both the economics and the emissions in supplying the demand, which is the focus of this paper. Figure 1 illustrates the overall approach and outline of the paper. While MES have classically been studied from the perspective of co-generation (Cogen or combined heat and power or CHP) and tri-generation (Trigen) processes as a way to enhance overall energy supply efficiency and economics, this paper considers a system of energy conversion and storage processes rather than a single device. More specifically, this paper considers the buildings and energy processes of a university campus and associated economic and carbon efficiencies. For a comprehensive overview of MES, please see [12].

The notion of (thermodynamically) flexible buildings in this manuscript refers to the concept that heating and cooling demand represents energy processes with (thermal) inertia that are inherently flexible. This is because the demand is specified by a building's ability to maintain thermal zones' temperature set-points within a (pre-specified) dead-band. Increasing the dead-band permits a shift in the building's demand across larger time-periods, which begets flexibility in building demand and permits greater economic efficiency. In addition to innovations on building efficiency and flexibility, there is also a growing popular demand for carbon tax policies, which alter the economics of energy. Within that context, this paper seeks to study and investigate the following question: *for a realistic MES, what role can flexible buildings play in reducing costs and emissions relative to a carbon tax?*

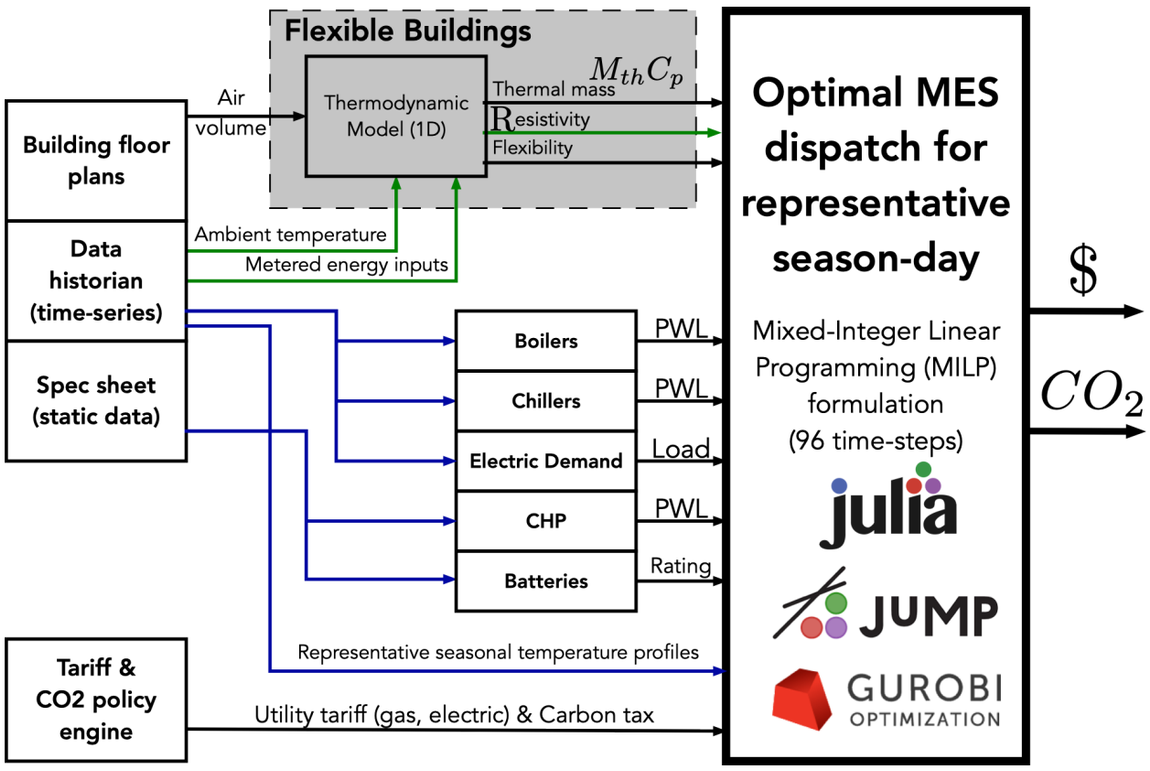

Figure 1: Summary of overall methods with necessary data and models to perform MES co-optimization of utility economics and carbon emissions by using flexible buildings and multi-energy processes.

To answer this question, we

1. analyze real data from buildings to develop a simplified, averaged first-order model of a thermodynamically flexible building;

2. develop a predictive model of a flexible MES, including nonlinear energy conversion processes inherent to realistic boilers, chillers, and combined heat and power plants;

3. optimize over the actual natural gas and electric energy and demand tariffs that promote "economic efficiency" and consider the role of a carbon tax; and

4. construct and analyze a realistic case-study based on data from University of Vermont in Burlington, Vermont in the northeastern United States.

Most of the early work on MES focuses on combined natural gas and electrical optimal power flow (or GEOPF) on multi-carrier networks [13, 14]. This early work on MES optimization established the existence of new minimum cost solutions that were not achievable when studying the energy systems in isolation. In addition, these methods led to the MES modeling frameworks of so-called "Energy Hubs" and "Power Nodes" [15, 16, 17, 18] . The energy hub framework has enabled past interesting studies in: distributed control of energy hub systems, impact of hybrid-electric transportation, integration of energy storage, and multi-energy analysis of buildings [19]. Generalizing the energy hub models to manage flexible buildings as part of a MES has been presented, including [20], but was focused on

control and short term operations rather than emissions and planning problems, which is the focus in the current paper.

Herein, we build on concepts from university campus-scale MES [10], which developed a piece-wise linear (PWL) framework and illustrated the value of considering the nonlinear energy conversion processes of boilers, chillers and combined heat and power (CHP) assets. In this current paper, we employ a similar PWL approximation of the underlying nonlinear energy efficiencies. However, the PWL approaches now more accurately capture the energy processes and we augment energy storage with available energy flexibility from buildings by allowing the buildings' internal temperatures to deviate from their set-points. Much of the literature on flexible buildings focuses on feedback control or online optimization over at couple hours or up to a day [21]. These works generally leverage historical MES demand data to construct seasonal electric, heating, and cooling demand profiles to build representative daily demand curves. In this paper, we also employ representative daily MES demand curves to study the impacts of flexibility and carbon taxes. However, we additionally use the historical MES data to identify the thermodynamic parameters for buildings to study thermal flexibility, in terms of the internal temperature set-points. Thus, the key contributions of this paper is the identification and integrating of flexible buildings within economic optimization of a nonlinear MES (time-coupled, PWL), and the analysis of comparing the effects of flexible buildings against that of a price on carbon emissions. Specifically, unlike very recent work from [18] that is also focused on campus-scale MES and carbon emissions within the context of an energy hub coordination scheme, we focus on how flexibility in the thermal demand together with a carbon tax can improve overall MES economics and CO2 emissions. While (thermodynamically) flexible buildings and virtual energy storage (VES) have been explored previously within the context of multi-stage, hierarchical optimization of microgrid operations and economics [7, 22, 23], these works do not consider the role of natural gas energy conversion processes and gas tariffs nor CO2 emissions. For work on MES microgrids that include emissions (but not necessarily carbon pricing policies), the literature tends to not consider larger dynamic buildings loads nor resources that require ramp-rate and start-up costs, since the focus is on small and nimble residential demand-side MES resources [24]. That is, the current paper shows that flexibility in the Vermont-based system (which has access to 100% renewable electricity from the utility) can achieve similar outcomes with flexibility that it can with a carbon tax. That is, the incentives of economic efficiency mostly align with those of the carbon tax in this system, which means that unlocking building-level flexibility in Vermont can lead to significant reductions in carbon without necessarily requiring an expensive carbon tax.

The outline of the paper is as follows: Section 2 presents the MES model for curating

the objective function and PWL constraints. The flexible buildings parameters are identified and estimated in Section 3 based on real demand and weather data. Section 4 presents the case-study on flexibility in Vermont, while Section 5 presents the conclusion and directions for future work.

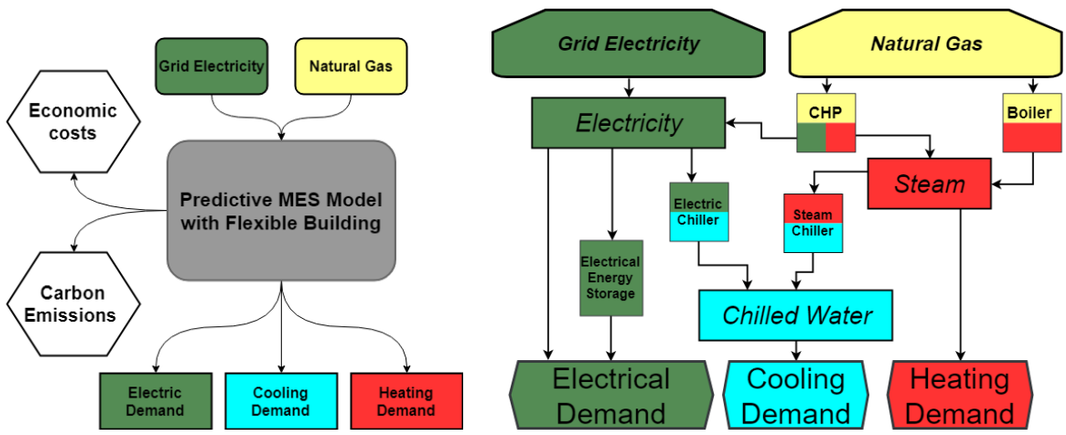

Figure 2: *Left*: System-level overview of the MES system considered in this paper with economic costs and emissions as the key outputs. *Right*: physical asset-level overview of the MES considered in this paper. The energy conversion processes are illustrated with color changes. Flexible buildings make up the cooling/heating demands at the bottom.

2 System Modeling

From Fig. 2, the proposed general MES framework is presented (on the left) and is separated into different physical blocks to represent devices and their physical energy conversion and storage processes (on the right). Each device modeled could be categorized in one of three block types: 1) source blocks, 2) storage blocks, and 3) conversion blocks. Source blocks are used to supply energy (at some potential cost), which includes natural gas and electricity. These blocks are used to calculate costs of operation as well as carbon emissions and are further discussed in Section 2.1. Storage blocks store energy over multiple time-steps and could represent electric batteries or thermal energy storage tanks whose general form is explained in Section 2.2. Conversion blocks represent devices, such as chillers, boilers and CHPs that transform one energy input into one or more energy outputs. Of course, these conversions are subject to the physical reality of energy losses, which begets inefficiencies that are described in Section 2.3.

The general problem formulation represents an offline day-ahead, multi-energy planning problem over a representative day (i.e., 24-hour horizon) at 15-minute resolution to capture $t = 1, \ldots, T$ timesteps, where $T = 96$. This problem is formulated by the following and

detailed in the next sections:

$$\text{minimize } f_{\text{el}}^{\text{cost}}(G_{\text{in}}^{\text{el}}) + f_{\text{gas}}^{\text{cost}}(G_{\text{in}}^{\text{gas}}) + f_{\text{CO2}}^{\text{cost}}(G_{\text{in}}^{\text{el}}, G_{\text{in}}^{\text{gas}}) \tag{1a}$$

$$f_{\text{el}}^{\text{conv}}(G_{\text{in}}^{\text{el}}, G_{\text{in}}^{\text{gas}}) = E_{\text{el}}^{\text{dem}}[t] + P_{\text{in}}^{\text{bat}}[t] - P_{\text{out}}^{\text{bat}}[t] \tag{1b}$$

$$f_{\text{th}}^{\text{conv}}(G_{\text{in}}^{\text{el}}, G_{\text{in}}^{\text{gas}}) = E_{\text{th}}^{\text{dem}}[t] \tag{1c}$$

$$E^{\text{bat}}[t+1] = E^{\text{bat}}[t] + \eta_{\text{in}} P_{\text{in}}^{\text{bat}}[t] - \frac{1}{\eta_{\text{out}}} P_{\text{out}}^{\text{bat}}[t] \tag{1d}$$

$$E^{\text{bat}}[T] = E^{\text{bat}}[0] \tag{1e}$$

$$\theta[t+1] = \theta[t] + \frac{\Delta t}{M_{th} C_p} \left((1 - \eta_{\text{use}} U[t])\, E_{\text{th}}^{\text{dem}}[t] - R \frac{(\theta[t] - \theta_{\text{amb}}[t])}{\Delta t} \right) \tag{1f}$$

$$\frac{1}{T} \sum_{t=0}^{t=T} \theta[t] = \theta_{\text{Set}} \tag{1g}$$

$$0 \leq E^{\text{bat}}[t] \leq E_{\text{max}}^{\text{bat}} \tag{1h}$$

$$0 \leq P_{\text{in/out}}^{\text{bat}}[t] \leq P_{\text{in/out}}^{\text{bat}} \text{max} \tag{1i}$$

$$\theta_{\text{Set}} - \frac{\theta_{\text{flex}}}{2} \leq \theta[t] \leq \theta_{\text{Set}} + \frac{\theta_{\text{flex}}}{2} \tag{1j}$$

Relations in (1) provide a high-level overview of an optimization formulation that allows us to understand how flexibility and carbon pricing affect overall energy costs. The energy costs f^{cost} in (1a), are defined via natural gas ($/MMBtu) and electric ($/kW, $/kWh) utility tariffs and carbon prices ($/lb) based on cumulative CO2 emissions. The energy consumed by the MES is converted, via nonlinear f^{conv} in (1b) and (1c), into heating, cooling, electricity components that either supply other conversion processes (e.g., co/tri-generation) or meet MES demand. However, if some demand is flexible, such as those enabled by electric batteries in (1d) or those enabled by smart buildings that can manage thermal loads over a greater time period as shown in (1f) with temperature θ. That is, the temperature and battery state of charge (SoC) limits in (1j) and (1h), (1i) represent the available flexibility range. Of course, sustainability constraints such as the ones in (1e) and (1g) ensure that over the prediction horizon of a representative day that the system is returned to the initial (energy) state. Note that additional constraints are added to (1) based on operational requirements described in Section 2.4, such as minimizing start-up events and limiting unnecessary ramping of conversion devices.

Now, in the next sections, we focus on defining and modeling the cost functions, nonlinear energy conversion and storage processes, and parameterizing the thermal flexibility models with limited data. Clearly, solving this nonlinear (and non-convex) optimization problem to optimality is computationally challenging, so we focus on a tractable piecewise-linear (PWL) approximation of the non-linearities to engender a mixed-integer linear program (MILP) formulation, which is solvable by today's MILP solvers and provides a bound on the

optimality gap.

2.1 Energy economics

Almost all systems are driven by economic incentives and MES are no different. That is, the focus on operating an MES is always on economic efficiency (i.e., costs), which is why carbon taxes put a price on carbon. At the core of these costs are utility tariffs from natural gas and electricity, which are described next and make up the objective function of the MES optimization problem described in this paper. These costs were pulled from the existing billing systems in place for both the electrical and natural gas tariffs. The billing and demand data collected is provided in English Inch-Pound (I-P) units, which is common for MES and HVAC systems in the U.S. [8, 25]. Key conversions from I-P units to SI units are provided in Table 1.

Table 1: Unit conversion table between English (I-P) and SI units.

Unit type	**English Unit (I-P)**	**SI Unit**
Temperature	1 degree change Fahrenheit (F)	$\frac{5}{9}$ degree change C
Power	1 Refrigeration Ton (RT)	3.517 kW
Energy	10^6 British thermal unit (MMBTU)	293.07kWh
Energy	1 Centum cubic feet (CCF) of natural gas	29.307 kWh

2.1.1 Natural gas

Natural gas is one of two energy sources available to the MES. The rate structure used in this model is from the energy plant's actual rate in Vermont and priced at \$0.8227/CCF, which relatively low as the rate is interruptible. Being interuptible means that during times of peak regional demand and limited supply (in the Northeastern U.S.), the MES can be forced to switch to fuel oil to reduce natural gas demand in the surrounding region. Since interruptions only occur for 1-2 weeks per year, it reasonable to simplify the MES and not consider fuel oil costs and impacts on boiler conversion efficiencies in this work.

Besides natural gas, the utility also offers the cleaner "renewable natural gas" (RNG). RNG represents natural gas made from methane that is extracted from landfills or livestock waste and fed into conventional natural gas pipelines. As a large consumer, the MES can hypothetically elect to purchase RNG at a fixed percentage of their total gas consumed every month: $\lambda_{\text{RNG}} \in \{10\%, 25\%, 50\%, 90\%\}$. For the sake of completeness, the cost and emission rates related to 100% RNG are provided in Table 2 and has the effect of an adder on natural gas rates. Clearly, any convex combination of conventional and renewable natural gas results in a convex combination of the costs and emissions. Thus, the cost of $G_{\text{in}}^{\text{gas}}$ CCF of gas with

RNG adder of λ_{RNG} is as follows:

$$f_{\text{gas}}^{\text{cost}}(G_{\text{in}}^{\text{gas}}) := \sum_{t=1}^{T} \left(0.8227(1-\lambda_{\text{RNG}}) + 1.174\lambda_{\text{RNG}}\right) G_{\text{in}}^{\text{gas}}[t]. \tag{2}$$

This represents a potentially bilinear expression, unless λ_{RNG} is fixed *a-priori* to a constant, which is what is done in this paper. Specifically, we set $\lambda_{\text{RNG}} = 0$ since RNG trades off directly with any carbon tax and does not engender any new insights into the MES problem.

Table 2: Natural Gas Rate Parameters

Name/ Info	**Value(s)**	**Unit**
Cost of conventional natural gas (NG)	0.8227	$/CCF
Cost of Renewable Natural Gas (RNG)	1.174	$/CCF
CO2 emissions from NG	11.71	lbs of CO2/CCF
CO2 emissions from RNG	5.01	lbs of CO2/CCF

2.1.2 Electricity

Besides natural gas, the MES has access to a second energy sources in the form of electricity from the utility Burlington Electric Department (BED). BED's power is supplied from a 50MW bio-mass generator, distributed solar PV, wind turbines, and hydro-power generation and imports, which makes BED's entire electric supply 100% certified renewable with no associated CO2 emissions. In fact, BED was the first utility in the U.S. whose supply was fully certified as renewable [26], which make the MES somewhat unique.

While the MES consists of multiple buildings and each building has its own electric meter and, depending on it size, its own electric rate, we have chosen to focus on the most common and higher priced primary service (or *Ps*) rate, which is described by on/off-peak hours in Fig. 3 and corresponding rates in Table 3. The *Ps* rate structure includes time-of-use (TOU) and seasonally varying energy ($/kWh) and demand ($/kW-month) charges. In addition, we include the standard fixed account fees and energy efficiency charges, as well as associated taxes. From historical data, the majority of the costs come from demand and usage charges, which can vary significantly over the year depending on months of the year and hours of the day. To compute the total MES electricity input costs from total usage (kWh over 15-minute intervals), $G_{\text{in}}^{\text{el}}[t]$, we have:

$$\begin{aligned} f_{\text{el}}^{cost}(G_{\text{in}}^{\text{el}}) :=& \frac{1}{4}\left(0.00413 G_{\text{in}}^{\text{el}}[t] + \sum_{t\in\text{on}} u_{\text{on}} G_{\text{in}}^{\text{el}}[t] + \sum_{t\in\text{off}} u_{\text{off}} G_{\text{in}}^{\text{el}}[t]\right) \\ &+ (d_{\text{on}} + 1.6614) \max_{t\in\text{on}} G_{\text{in}}^{\text{el}}[t] + (d_{\text{off}} + 1.6614) \max_{t\in\text{off}} G_{\text{in}}^{\text{el}}[t], \end{aligned} \tag{3}$$

where $u_{\text{on/off}}, d_{\text{on/off}} \geq 0$ represent usage and demand charges, respectively, during on/off-

peak periods ($t \in$ on/off) of the day for a particular season (winter, shoulder, or summer) per Table 3. Since we minimize demand charge rates that are strictly positive (with the efficiency adder), we can reformulate the max terms using an equivalent, linear formulation with an extra variable and additional inequality constraints:

$$\max_{t \in \text{on/off}} G_{\text{in}}^{\text{el}}[t] = \hat{G}_{\text{in}}^{\text{el}}[t], \text{ for } \hat{G}_{\text{in}}^{\text{el}}[t] \geq G_{\text{in}}^{\text{el}}[t] \ \forall t \in \text{on/off}.$$

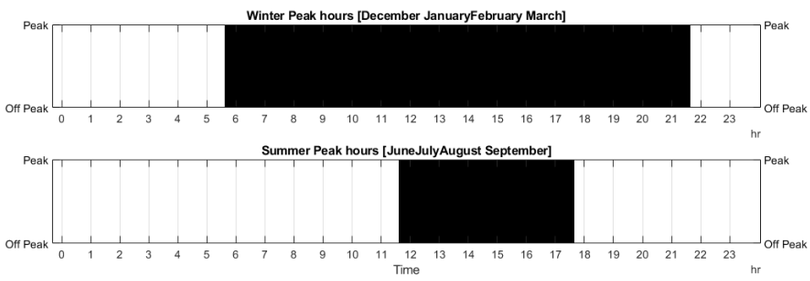

Figure 3: Peak hours begin at 6:00am and end at 10:00pm for the winter months while, for the summer, peak hours are from 12:00pm until 6:00pm. Shoulder months (April, May, October, November) are always under off-peak rates.

Table 3: Electric Rate Parameters

Description	**Value(s)**	**Unit**
Energy efficiency demand	1.6614	\$/kW-month
Energy efficiency usage	0.00413	\$/kWh
Peak demand (winter, shoulder, summer)	[25.17, 0, 25.17]	\$/kW-month
Peak usage (winter, shoulder, summer)	[0.103813, 0, 0.095552]	\$/kWh
Off-peak demand charges	3.45	\$/kW-month
Off-peak usage charges	0.067251	\$/kWh
CO2 emissions from electricity	0.0	lbs of CO2/kWh

2.1.3 Carbon Emissions

To understand and compare how flexibility and carbon-taxes affect the overall economics, we need to assign a price to carbon (\$/lb-CO2). Based on recent climate change and energy policy discussions in Vermont (U.S.) and globally, the price is predicted to become anywhere from \$100-5,500/ton-CO2 [2, 27] by 2030, which is the range from which we choose our carbon tax rates for this MES. Thus, the carbon emission costs are added to $f_{\text{gas}}^{\text{cost}}(G_{\text{in}}^{\text{gas}}) + f_{\text{el}}^{\text{cost}}(G_{\text{in}}^{\text{el}})$ via the following:

$$f_{\text{CO2}}^{\text{cost}}(G_{\text{in}}^{\text{el}}, G_{\text{in}}^{\text{gas}}) := C_{CO2}^{\$} \left(\sum_{t=1}^{T} 0.0 G_{\text{in}}^{\text{el}}[t] + 11.71 G_{\text{in}}^{\text{g as}}[t] \right), \tag{4}$$

which completes the objective function description. Next, we describe models and constraints related to energy storage and conversion processes.

2.2 Energy storage processes

Energy storage processes can be in the form of thermal energy storage (e.g., ice-storage, heated rocks, molten salt) and chemical energy storage (e.g., Lithium-ion electric batteries). In this paper we focus on electric batteries. Later, we will also describe flexible buildings as part of the demand, however, energy flexibility is another source of energy storage that we leverage in this work, but is not described in this section.

2.2.1 Energy storage model

The main purpose of energy storage is to shift demand in time. For example, both the grid and the (local) CHP can supply energy storage during charging. Due to the daily cycling, we assume no standing losses. Thus, energy storage devices are modeled as follows.

Let $E^{\text{bat}}[t]$ denote the state of charge (SoC) of the battery at time-step t. There are two different conversion processes that incur energy losses associated with operating the storage device: (1) losses while charging, η_{in}, at charging rate $P_{\text{in}}^{\text{bat}}[t]$ and (2) losses when discharging, η_{out}, at discharging rate $P_{\text{out}}^{\text{bat}}[t]$. From these terms, we can model the discrete-time (first-order) dynamics of the SoC relative to charging and discharging rates and the energy capacities, $E_{\text{max}}^{\text{bat}}[t]$ of the storage device over prediction horizon $t \in [0, 1, \ldots, T]$:

$$E^{\text{bat}}[t+1] = E^{\text{bat}}[t] + \eta_{\text{in}} P_{\text{in}}^{\text{bat}}[t] - \frac{1}{\eta_{\text{out}}} P_{\text{out}}^{\text{bat}}[t], \tag{5}$$

$$0 \leq E^{\text{bat}}[t+1] \leq E_{\text{max}}^{\text{bat}}. \tag{6}$$

In addition, there are charging and discharging rate limits, R^{bat} on charge/discharge powers. These vary for each device and limit the amount of power supplied to or consumed from the grid per time step: $0 \leq P_{\text{in}}^{\text{bat}}[t] \leq R^{\text{bat}}$ and $0 \leq P_{\text{out}}^{\text{bat}}[t] \leq R^{\text{bat}}$.

Finally, we enforce a sustainability condition on energy storage to ensure consistency between representative periods in the simulation. This condition ensures that the initial energy states and terminal energy states of the device are the same: $E^{\text{bat}}[0] = E^{\text{bat}}[T]$. Table 4 outlines the battery specifications used in this paper.

Remark (Simultaneous battery charging and discharging)**.** *Note that while the formulation for the battery model above permits a feasible solution with simultaneous charging and discharging (i.e., $X_{SCD}[t] := P_{in}^{bat}[t] P_{out}^{bat}[t] \geq 0$), the strictly positive prices for electricity guarantee that, at optimality, $X_{SCD}[t] \equiv 0, \forall t$ as long as the original problem is feasible [28]. For details on simultaneous charging and discharging, please see [29]. Thus, it is not necessary to create a separate binary variable to indicate charging/discharging to ensure physically realizable battery dispatch.*

Table 4: Battery Parameters

Parameters	**Value**
Battery capacity, $E^{\text{bat}}_{\text{max}}$	308 kWh
Max power rate, R^{bat}	77 kW
Battery charging losses, η_{in}	95%
Battery discharging losses, η_{out}	95%

2.3 Energy conversion processes

Energy conversion processes, defined generally by $f^{\text{conv}}_{\text{el/th}}$ in (1) map energy inputs to energy outputs for the boilers, chillers, and CHP. Converting energy from natural gas to steam or to electricity and from steam or electricity to chilled water for cooling loads is a process with which there are associated energy losses (i.e., inefficiencies). These energy losses depend on the assets and their operations. For example, operating two natural gas steam boilers (natural gas to steam) at low load relative to one at high load can yield significant efficiency improvements. Many plants operate under so-called "$N + 1$ mode" where if any boiler or chiller were to fail, the remaining devices could pick up the slack. While these constraints could be added, they have been ignored in this work to focus on the relationship between flexible demand and economic efficiency and carbon emissions. First, we describe the two main thermal energy conversion processes (steam and chilled water) before providing their input-output models and the piecewise linear (PWL) formulation employed in this paper.

2.3.1 Generating steam

The boilers and CHP employ combustion to convert natural gas to steam. The main difference between the two blocks lies with the CHP doing the conversion indirectly. Specifically, the CHP combusts natural gas (with compressed air) to create hot, high-pressure gas, which propels a gas turbine to drive an AC generator that converts mechanical energy to electricity. The resulting hot exhaust gas from the turbine is then used along with a heat-exchanger to generate steam [30]. As shown in Table 5, the boiler's steam output is a nonlinear, non-convex function of the natural gas input while the CHP's steam output is assumed to be a linear function of the gas input (since steam is a byproduct of electric generation). This means the CHP generates steam at constant efficiency. Specifically, in Table 5, the boiler's nonlinear steam efficiency varies from 36-93% depending on the asset's loading (i.e., output). The CHP is assumed to have a constant steam conversion efficiency of 53%. However, after their normalized inputs exceeds 20% of their range, the boiler is the most economical choice for supply thermal demand.

For simplicity and owing to the planning purposes in this paper, we have chosen to ignore the complexities of mass flow rates of flues, steam loops, electric pumps, and air compressors

and instead focus on the input-output relations between the different assets. Similarly, if steam is needed for a process, such as the steam-driven chiller (described next), it is assumed that operations ensure that steam is at the desired temperatures and pressures. Finally, we relax the MES operators' standard procedure and allow boilers and CHP to vent. This will permit the CHP to provide (valuable) electricity without requiring a steam host, which is a challenge in Summer time when demand charges are greatest and it's too warm for a heating load. Since the price of natural gas is positive and the objective function includes natural gas cost terms, venting will only occur sporadically.

2.3.2 Chilled Water Generation

There are two different types of chillers used in the model, electric and absorption chillers. The electric chiller converts electricity to chilled water while the absorption chiller converts steam input to chilled water output. Both devices operate in a similar manner besides the different inputs and have the same general operating assumptions. For each of them, heat transfer between the condenser, evaporator and cooling towers are neglected. Instead, energy in and out are considered with a variable efficiency based on the device's coefficient of performance (COP). That is, as was done with boilers and CHP, we have neglected the chilled water mass flows, pumps, and valves and deal solely with energy flows and lumped thermal demands, which is reasonable for the planning purposes of this paper.

Next, we describe the input-output relations of these devices and formulate the piece-wise linear (PWL) model to turn the nonlinear, non-convex efficiency curves into a computationally tractable formulation (albeit by introducing integer variables). Nonetheless, given the maturity of Mixed integer Problem (MIP) solvers and the underlying MILP formulation, we can solve to (near) optimally as will be discussed in the results section.

2.4 Piece-wise linear (PWL) formulation

Energy conversion processes, such as $f^{\text{conv}}(.,.)$ from (1b) and (1c), are generally nonlinear and non-convex. To ensure a formulation that has a tractable global (near) optimal solution and outperforms the overly simplified assumption of a constant efficiency, we follow the work in [10] to replace the nonlinear input-output curves with their PWL approximations. The empirical[1] nonlinear, normalized input-output curves are provided in Table 5 for energy conversion processes employed by the MES. When there are multiples of the same device type, the performance curves have been de-rated slightly to differentiate their dispatch.We have used the linear input-output model described in [3] for modeling chillers and the CHP's heat recovery steam generator. This simplifies the formulation but also engenders good

[1]The input-output curves are a function of historical performance data and original manufacturer data.

quality models[2]. That is, while the PWL framework offers superior generalizable modeling capability over other linear formulations by being able to capture non-monotonic efficiency curves, it also increases computational complexity significantly. Thus, Table 5 is designed based on trading off modeling accuracy and computational complexity.

Table 5: Input (X) to output (Y) performance curves

Device	Normalized Performance curve (based on [10])
Boiler	$Y = -3.797X^4 + 5.422X^3 - 1.087X^2 + 0.162X$
CHP (to Electric)	$Y = 0.362X^2 + 0.609X$
CHP (to Steam)	$Y = 0.966X$ ($R^2 = 0.968$)
Absorption Chiller	$Y = 1.087X - 0.062$ ($R^2 = 0.998$)
Electric Chiller	$Y = 1.206X - 0.130$ ($R^2 = 0.988$)

To generate the PWL approximation, we mostly follow [10] by first defining the maximum input/output operating ranges for each device. The original nonlinear curve is limited between those operating points. Next, we select $M+1$ input-output pairs from the nonlinear curve, which define M PWL segments. Each PWL segment or bin $i = 1, \ldots, M$ is defined by a linear expression consisting of a slope, m_i and an intercept b_i: $Y = m_i X + b_i, \forall i = 1, \ldots, M$.

Thus, at time t and for each device, the input, $X[t]$, and output, $Y[t]$, variables are created. Each device also has static input limits $X_{\min}$ and $X_{\max}$, as well as a ON/OFF states, $X_{\frac{1}{0}}[t] \in \{0, 1\}$. If the asset is ON, then (7) ensures that it operates within its limits, while (8) ensures that the asset does not exceed a pre-defined static ramping limit, X_{ramp}:

$$X_{\min} X_{\frac{1}{0}}[t] \leq X[t] \leq X_{\max} X_{\frac{1}{0}}[t] \tag{7}$$

$$X[t] - X[t-1] \leq X_{\text{ramp}} \tag{8}$$

$$X_{\text{start}}[t] \geq X_{\frac{1}{0}}[t] - X_{\frac{1}{0}}[t-1], \tag{9}$$

where (9) tracks startup events with $X_{\text{start}}[t] \geq 0$, which incur a one-time, non-trivial startup energy penalty, $c^{\text{cost}}_{\text{start}}$ that is added to the objective function as $\sum_{t=1}^{T} c^{\text{cost}}_{\text{start}} X_{\text{start}}[t]$.

From the PWL setup, we now need to segment the input and output variables. Starting with the input, we define $X[t]$ as a collection of M bins, $B_i[t]$, that span the input range:

$$X[t] = \sum_{i=1}^{M} B_i[t]. \tag{10}$$

In (10), the binning of the input is achieved by introducing the binned input variables, B_i for PWL segment $i = 1, \ldots, M$. Recall, these M segments are generated from the nonlinear curve ranging from the minimum operation of the device to the maximum. However, to ensure that at most one input bin is active to represent the admissible input range of segment

[2]By "good model" we mean that the coefficient of determination satisfies $R^2 > 0.95$ compared with the full nonlinear model from data.

i, we need to limit the number of active bins to at most one:

$$\sum_{i=1}^{M} B_{\frac{1}{0},i}[t] \leq 1, \tag{11}$$

where $B_{\frac{1}{0},i}$ is the binary (0/1) segment indicator variable for PWL segment i. This ensures that the device is either OFF or operating within its input range and at the efficiency determined by the active PWL segment i.

Next, the binary segment indicator values are used to capture the admissible range of input bin $B_i[t]$ with the segment's upper and lower limits:

$$B_{\frac{1}{0},i}[t]\underline{B_i} \leq B_i[t] \leq B_{\frac{1}{0},i}[t]\overline{B_i}. \tag{12}$$

Note that these upper and lower segment bounds are defined by the consecutive input point pairs that make up PWL segment i. Finally, with PWL segment i's input range defined, we can define the output in terms of the input bins and the PWL segment line expressions as:

$$Y[t] = \sum_{i=1}^{M} m_i B_i[t] + B_{\frac{1}{0},i}[t]b_i \tag{13}$$

which ensures that that the output Y is always represented by a single active PWL segment (or none at all, if all binary segment indicator variables are zero). Figure 4 presents an example for a PWL approximation of a nonlinear, input-output curve with $M = 4$ segments.

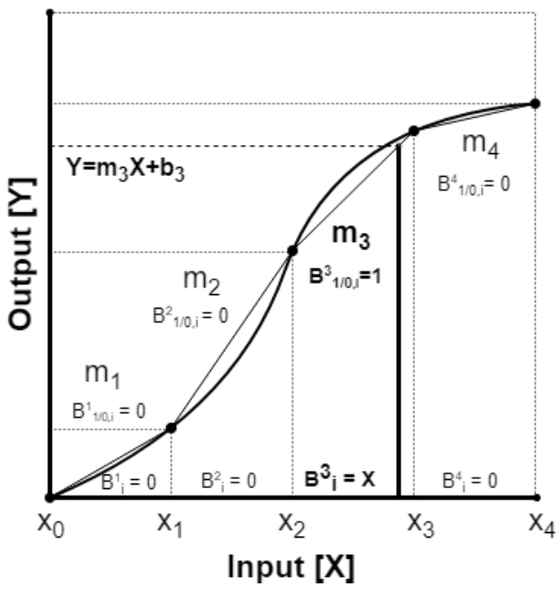

Figure 4: Example of using the PWL approximation for a general device with $M = 4$ segments and the corresponding input bins and binary segment indicator variables. Note that the third segment is active in this example (i.e., $B_{\frac{1}{0},3} \equiv 1$).

2.5 Demand

Through the energy storage and conversion processes, the goal of any MES is to supply the (multi-energy) demand while minimizing economic costs as illustrated in Fig. 2. In this section, we describe the demand types and highlight the nature of the flexibility in thermal (building) demand.

2.5.1 Electric Demand

Three years of electrical demand was recorded from the meters of each building and aggregated to create one representative weekday and weekend-day for each month. The representative weekdays are illustrated in Figure 5. From these representative seasonal days, we can construct the seasonal weeks and months.

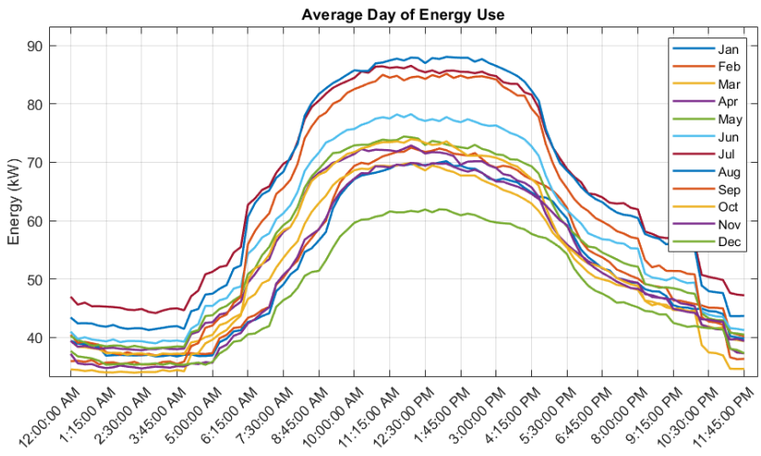

Figure 5: Average weekday electricity usage per month

To meet the electric demand, electricity is either supplied by the grid E^{Grid} (subject to the electric rate) or generated in via a CHP E^{chp} (subject to conversion process and natural gas rate). The electricity supply must satisfy the electric demand, E_d^{Tot} (from Fig. 5), any net demand from the battery $P_{\text{in}}^{\text{bat}}[t] - P_{\text{out}}^{\text{bat}}[t]$, and any electric chiller demand, $E_{\text{Chw}}^{\text{Tot}}$. That is, the electric power balance requirements is:

$$E^{\text{chp}}[t] + E^{Grid}[t] = P_{\text{in}}^{\text{bat}}[t] - P_{\text{out}}^{\text{bat}}[t] + E_d^{\text{Tot}}[t] + E_{\text{Chw}}^{\text{Tot}}[t]. \tag{14}$$

2.5.2 Thermal building flexibility

Unlike the electrical demand, there is no single meter from which to measure heating and cooling demand directly. That is because heating and cooling demands are a function of the desired level of comfort (i.e., temperature set-points within a building). This temperature fluctuates around the set-point by a few degrees during conventional thermostatic operation. By allowing larger temperature deviations around the set-point, there is greater flexibility in supplying the thermal demand, which intuitively should improve the

MES economic efficiency, if comfort levels are not significantly impacted. Thus, flexibility and thermal (heating/cooling) demands are closely intertwined. As the buildings' temperatures, θ_{set}, and the ambient temperature, θ_{amb}, change, the building requires either a supply or removal of heat from the building. Specifically, the thermal flexibility of a building refers to the allowable temperature range, i.e., high thermal flexibility implies a large temperature range.

In this model, we employ ambient temperature data available from the local airport and this data was averaged in a similar manner to the electrical data to provide a representative dataset for each month. This data set was then used together with the building management system's (BMS's) set-point and a one-dimensional heat transfer model approximation of the building to model heating, cooling, and ambient thermal losses. The model then assumes that the set-point temperature was maintained close to the BMS's set-point, which together with ambient temperature data and the energy supplied to the building gives us a reasonable approach to estimate thermodynamic parameters of the buildings. Specifically, (15) relates the net energy supplied to the building, $E_{\text{in}}[t]$, to the demand-serving assets (heating or cooling) for a given time period t. Boilers and the CHP can separately supply steam for heating, S_d^{Tot}, increasing the building's temperature while chillers supply chilled water (cooling), $\text{Chw}_d^{\text{Tot}}$, to decrease the temperature in the building. The thermal building energy balance equation is

$$E_{\text{in}}[t] = S_d^{\text{Tot}}[t] - \text{Chw}_d^{\text{Tot}}[t], \tag{15}$$

where total steam is supplied by the boilers and CHP and total cooling is supplied by the two different chiller types. Of course, the absorption chiller allows the steam generated to be used for cooling instead.

To compute $E_{\text{in}}[t]$ for a building, we need to map $E_{\text{in}}[t]$ to the average building temperature dynamics and, thus, require a heat transfer model [31, 32, 33]. This is given by the following:

$$\frac{M_{th}C_p(\theta[t+1]-\theta[t])}{\Delta t} = (1-\eta_{\text{use}}U[t])\,E_{\text{in}}[t] - R\,(\theta[t]-\theta_{\text{amb}}[t]) \tag{16}$$

$$\Rightarrow \theta[t+1] = \theta[t] + \frac{\Delta t}{M_{th}C_p}\left((1-\eta_{\text{use}}U[t])\,E_{\text{in}}[t] - R(\theta[t]-\theta_{\text{amb}}[t])\right). \tag{17}$$

On the left-hand side is the building's temperature θ and thermal mass M_{th}, while the right-hand side contains the energy input from the MES E_{in}, as well as added/lost heat due to ambient forcing term, θ_{amb}, and uncontrollable building occupancy parameter, $U[t] \in \{0, 1\}$. The occupancy parameter $U[t] = 1$ when the building is open/operational; else, $U[t] = 0$. That is, $\eta_{\text{use}}U[t]$ represents an approximation of the impact of human activity on the building energy usage (e.g., increased energy loss from opening/closing windows). The terms M_{th},

C_p, R, and η_{use} are further explained in Table 9 and detailed in Section 3, where they are identified from historical demand and weather data.

Remark (First-order models)**.** *The first-order thermodynamic approximation of a building is deemed reasonable in this context due to: i) the high-level, planning objectives of the MES predictive, optimization problem; and ii) since demand data represent averaged monthly weekdays and weekends. Furthermore, prior works in literature on building models and validation have concluded that first- and second-order models are sufficiently accurate input-output representations of buildings [31].*

One of the key contributions of this paper is the parametrization of a flexible building, which includes the ability of the building to operate within a dead-band around the BMS's temperature set-point. The larger the dead-band, the more flexibility the building has. This allows the building to behave similarly to a thermal energy storage device. The building can be charged by raising or lowering the temperature relative to the ambient temperature, and then discharge by not supplying as much heating or cooling and allowing the indoor temperature move towards the upper or lower dead-band bound (depending on the season). This can allow for preheating or pre-cooling based on a predicted increase in demand, change in ambient temperature, or to reduce peak demand. In (18), and (19), the temperature bounds and the averaging constraint on temperature excursions from the set-point ensure that the comfort levels are satisfied on average;

$$\theta_{\text{Set}} - \frac{\theta_{\text{flex}}}{2} \leq \theta[t] \leq \theta_{\text{Set}} + \frac{\theta_{\text{flex}}}{2}, \tag{18}$$

$$\frac{1}{T}\sum_{t=1}^{t=T} \theta[t] = \theta_{\text{Set}}. \tag{19}$$

In this paper, we will consider different scenarios where the dead-band is based on $\theta_{\text{flex}} \in \{1, 3, 5, 10, 20\}^{\circ}\text{F}$, but that over the course of the day, the average temperature must be equal to the set-point, which ensures that average comfort is met. As with energy storage, we impose a terminal consistency constraint on the temperature that, together with the above constraints, ensure that comfort is achieved on average and that every day starts and ends at the same temperature set-point: $\theta[0] = \theta_{\text{set}} = \theta[T]$. Next, we use building data to estimate parameters that define a flexible building.

3 Identifying flexible building parameters

3.1 One Dimensional Heat Transfer Model Parameters

The first-order thermal building model introduced in (17) assumes a single wall with a thermal resistance and a mass of air on one side at ambient temperature and a mass of air on the other side equal to the equivalent thermal mass inside the building. To use this model, we need to approximate the model parameters ($M_{\text{th}}C_p$) and R. Sections 3.1.1 and 3.1.2 discuss how these parameters are estimated from building data.

3.1.1 Approximating thermal mass: $M_{th}C_p$

To determine the thermal mass for the model, data was collected for the total available building space, e.g., please see Table 6. The number of floors, rooms, wall height and thickness as well as the floor space and its usage were documented. Gross floor space encompasses all usable and structural floor space. Assignable and Non-assignable areas are differentiated by where normal building usage can (e.g., office space) and cannot take place (boiler room and HVAC attic space). The Usable floor space is the summation of Assignable and Non-assignable floor-space. While this is a large space, it mostly represents university administrative offices, which is not an intense (thermal or electric) load. In addition, the space has undergone numerous (static) energy effiency improvements.

Table 6: Building Data

Space	**Gross**(ft^2)	**Usable**(ft^2)	**Assignable** (ft^2)	**Non-assignable**(ft^2)
Total	243,519	207,853	131,558	76,295

Using this data, we were able to determine the total volume of air within these buildings, and convert to a thermal mass of air using its density. Walls, windows, doors and air vents are all lumped together in the thermal resistance term, R, which is approximated next.

3.1.2 Identifying thermal resisitivity parameter: R

The 1D approximation used for the building heat transfer model not only simplifies the temperature dynamics and optimization, but also the required set of model parameters. Thermal resistivity is needed to calculate the energy transfer between the buildings to the ambient surroundings. Using heat transfer relation in (16), it is reasonable to assume that under conventional building operation that the indoor temperature throughout the day is small (i.e., $(\theta[t+1] - \theta[t]) \approx 0$, which allows us to drop the left-hand side of (16) and get:

$$0 \approx E_{\text{in}}[t] - R(\theta[t] - \theta_{\text{amb}}[t]) \tag{20}$$

This form then states that the losses must be equal to the energy added, as there is no change in temperature inside the building. From this we can then solve for the thermal resistivity R in terms of the energy in (which we have from metered data) and the difference in temperature inside the building (i.e., the BMS's set-point) and ambient conditions (i.e., data from the local airport):

$$R = \frac{E_{\text{in}}[t]}{(\theta_{\text{Set}}[t] - \theta_{\text{amb}}[t])}. \tag{21}$$

From the available metered interval data we can then set up a large set of equations and estimate R. Figure 6 shows the distribution of calculated R values for 7 months of data.

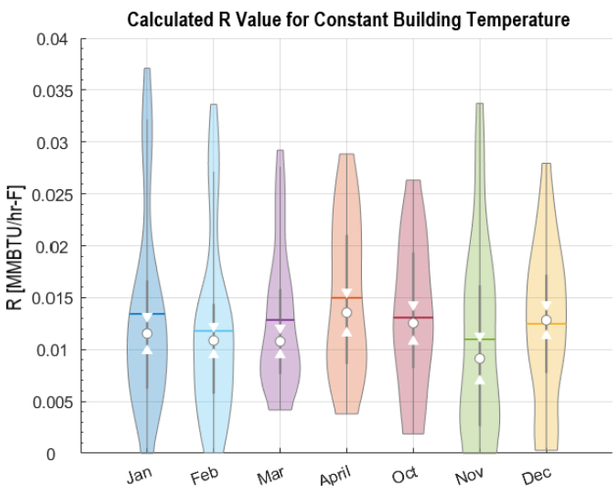

Figure 6: Distribution of estimated thermal resistivity R for different seasons based on data.

Interestingly, the mean values of R are consistent across the different months and we are focusing on an annual average outcome in the simulations, we average the monthly averages for the 7 months of estimates. This yields an average $R = 0.0139$ MMBtu/hr-F. Note that the standard deviation of the distribution of monthly R-values is within $\pm 10\%$ of the nominal R values for each month, i.e., $R \in [0.0125, 0.0153]$. Ongoing research is studying how to: (a) improve the estimate of R with time-series temperature data and (b) robustly optimize energy delivery to a flexible building under parametric uncertainty as in [34, 35].

3.1.3 Estimating building usage term, η_{use}

At a university, there can be a significant difference in utilization of the campus buildings between seasons (e.g., holidays, summer break, teaching semesters) and weekdays and weekends (e.g., lectures are on weekdays). This led us to consider estimating a correction factor for increased/reduced building utilization during day/night and weekend/weekday and gave rise to the notion of the building usage term, $U[t]$, which is a time-dependent binary parameter and not a variable that reflect internal building usage and corresponding energy usage disturbances (or losses) to account for the additional individuals and activity within the building during semester weekdays as well as the reduction during nights and weekends

outside of teaching semesters.

On average, ambient temperatures are similar for a representative weekday and weekend in a given season, so the only real change between these periods is building activity. A similar change can be found between daytime and nighttime however nights consistently have lower temperatures. In a given season, the temperature setpoints are also held constant by the BMS. This means that the same setpoint is used during the day and night as well as weekday and weekend. Thus, from steam flow and pressure data, as well as, the corresponding ambient temperature data collected over the past five years, we separated the data into into day and night bins and also weekday and weekend bins, which led to four data classes and clusters.The usage term can then be approximated from the centroids of each of the four day-time cluster, which are shown in Tables 7 and 8 for steam pressure and steam flow. For day and night, there are a larger temperature drops as well as a smaller drops in the usage term. Between weekday and weekend daytime usage there is a much smaller drop in temperature but still a noticeable change in usage.

Table 7: Centroids for steam pressure

Day-Time	**Pressure (psi)**	**Temp (F)**
Weekend-Night	954.84	47.05
WeekDay-Night	963.37	47.20
Weekend-Day	965.93	51.17
WeekDay-Day	969.75	52.03

Table 8: Centroids for steam flow

Day-Time	**Flow**	**Temp (F)**
Weekend-Night	7.54	47.05
WeekDay-Night	7.51	47.20
Weekend-Day	7.51	51.17
WeekDay-Day	7.42	52.01

From this we can estimate that the effect of the internal building activity (not energy usage) during the weekday leads to approximately $\eta_{\text{use}} = 1\%$ more energy consumed than for inactive times at the same temperature. This may be due to doors and windows being opened as well as more rooms being occupied and requiring additional energy to support. To be clear, this loss term is only present during weekday and day-time hours of the simulations and represents an additional (small) forcing term on the buildings to account for increased activity (relative to other times/days).

Combining the estimates of building parameters allows us to complete our flexible building parametrization, which is presented in Table 9. Next, we combine the MES model presented above with the flexible building model presented here to look at the high-level role that flexible buildings can play on MES and compare it to that of a carbon tax.

Table 9: Heat-transfer parameters for building

Parameter	**Value(s)**
Heat capacity of air, $M_{th}C_p$	0.3 MMBTU/F
Thermal resistance, R	0.01392 MMBTU/hr-F
Usage energy loss term, η_{use}	0.01
Usage time steps, U_{use}	Weekdays: 8am-10pm
Temperature range (flexibility), θ_{flex}	[1, 3, 5, 10, 20] F

4 MES case-study: economics & flexible buildings

Combining the models above with representative data and utility energy supply rates, we performed a number of tests for different scenarios of the available flexibility and carbon tax. The MES depicted in Fig. 2 is composed of two electric chillers, two absorption chillers, one large electric battery, one CHP, and two steam boilers. Each energy conversion process is represented by $M = 4$ PWL segments, except for the four chillers and the CHP's steam supply, which are all represented accurately with a single linear segment. The building temperature set-point was set to 70°F for all seasons since the set-points are not updated for different ambient conditions, seasons, or occupancy. Each season is represented by a month from summer (July), winter (January), and shoulder months (November), and the seasonal month is composed of representative weekdays (×22) and weekends (×8).

Five different flexibility levels are considered:

$$\theta_{\text{flex}} \in \{1(\text{none}), 3(\text{low}), 5(\text{medium}), 10(\text{high}), 20(\text{extreme})\},$$

and tested under four carbon pricing ($/ton-CO2) scenarios: $0, $100, $150, and $2000 per ton-CO2. While these carbon prices go beyond the political realities today, they are in line with recent UN reports and recommendations that range from $135-5500 per ton-CO2 [2].

The MES model is then cast as a mixed-integer linear program (MILP) with a representative season-day electric load and temperature profile that has a time-resolution of 15 minutes (i.e., 96 time-steps). Note that this model has about 2000 binary variables that are coupled temporally and spatially due to batteries, thermal flexibility, ramp-rate constraints, start-up costs, and It is implemented with Julia (v6.4.1) in JuMP (v.0.18.5) with GUROBI (v8.1) with a 1800 second time or 0.3% optimality gap solver limit imposed for each representative run. With five flexibility conditions, four different carbon prices, two representative days per season, and three seasons, the results represent 120 different MILP solutions.. The simulations were conducted on an Intel core i7 laptop with 16GB memory. All solutions presented are certified to be within 3.86% of the globally optimal solution with an overall average optimality gap below 0.6%, which is reasonable in the context of the averaged seasonal representative periods and model approximations.

Remark (MIP Gap)**.** *To be clear, the MIP Gap represents an upper bound on the optimality gap between the solver's integer-relaxed solution and the best integer-feasible solution. This means that a solution may indeed be globally optimal (but not provably so) and still have a MIP Gap* $> 0\%$*. Thus, the MIP Gap reflects a certificate of optimality more than an optimality gap for a pre-determined solver time limit.*

In that context, Table 10 lists the average MIP Gap for all (season, flexibility) pairs

over the four carbon price and two day-of-week scenarios. The Winter and Shoulder months generally achieve solutions that are well within the 0.3% limit of the global optimum before the 1800-second limit is up, which is the time limit imposed on the solver in this work. The Summer period represents a more complex system as the boilers and CHP can supply the steam-driven chillers that tightly couples multiple energy conversion processes and cost variables and leads to solution pairs that are within 2.7% of the global optimum after 1800 seconds. Note that from the results, we find that the objective function (that combines energy and CO2 costs) reduces monotonically as flexibility increases, which is what is expected from globally optimal solutions and indicates that the MIP-Gap is unlikely to have a significant impact on the conclusions.

Furthermore, given that the Winter and Shoulder solutions have very small MIP-Gaps, the occupancy correction factor, $\eta_{\text{use}} = 0.01$, in the model seems useful. For the Summer solutions, the larger MIP-Gap makes it unclear exactly how strongly the occupancy correction factor affects the solution.

Table 10: Solver MIP-Gap (%) for different flexibility and seasons

Flex	**1**	**3**	**5**	**10**	**20**
Winter	0.14	0.19	0.24	0.22	0.15
Summer	0.25	1.03	2.33	2.69	1.53
Shoulder	0.15	0.14	0.15	0.18	0.16

Figures 7-9 show the simulation results for an average day in each representative season: the forecasted operating costs and carbon emissions resulting from each flexibility, θ_{flex}, and carbon price scenario. The left figures represent the cost and emissions as flexibility increases. Across all left figures, the costs and emissions decrease with increased flexibility for the \$0/ton-CO2 price scenario. This is due to improved economic efficiency which aligns with reduced emissions in this Vermont system with access to 100% carbon-free electric utility service. Note that these result also highlight how this MES is limited in its ability to supply heating demand from the electric grid. This inflexibility in energy conversion is illustrated in Winter (Fig. 7(Left)) and Shoulder (Fig. 9(Left)) seasons with savings and emissions that are relatively insensitive ($< 1.5\%$) to building flexibility and carbon pricing. Only under extreme \$2000/ton-CO2 pricing (not visualized in the left figures) is it optimal for operators to shut OFF the CHP and procure electricity from the grid and bring ON a second boiler. This is shown in Figs. 7(Right) and 9(Right) with a large increase in grid imports and reduction in gas imports for only the most extreme carbon pricing scenario. The resulting cost increases are in the range of 60-230% with a reduction in CO2 emissions of 38%-55%.

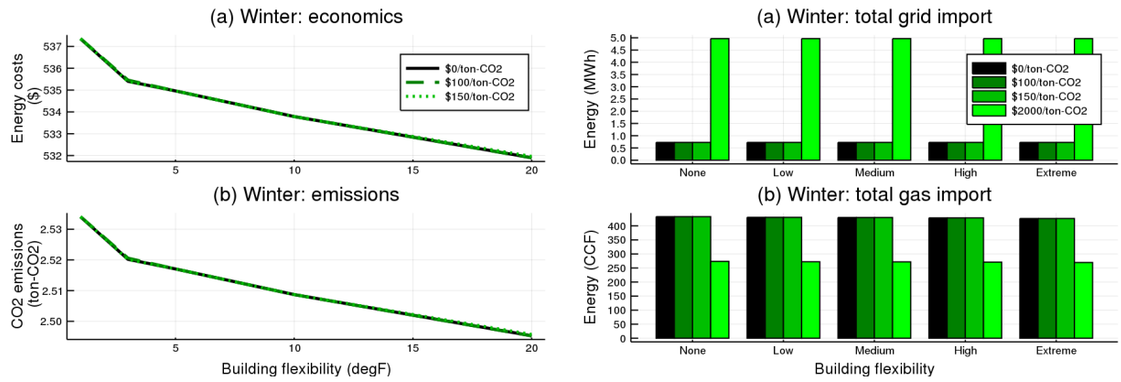

Figure 7: Simulation results for an average Winter season day for different levels of flexibility and carbon prices. *Left*: Energy costs and resulting emissions to understand (a) economics and (b) emissions. *Right*: energy imported from (a) grid and (b) gas pipeline suppliers to understand effects of flexibility and carbon prices.

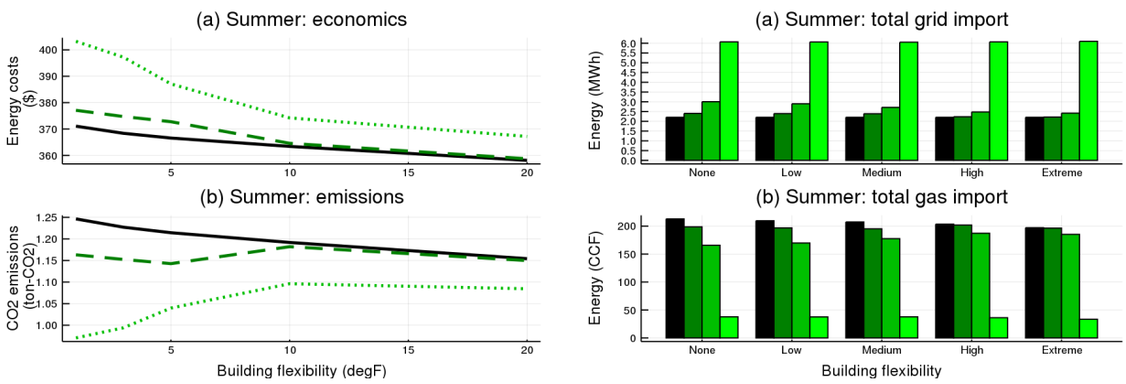

Figure 8: Simulation results for an average Summer season day for different levels of flexibility and carbon prices. *Left*: Energy costs and resulting emissions to understand (a) economics and (b) emissions. *Right*: energy imported from (a) grid and (b) gas pipeline suppliers to understand effects of flexibility and carbon prices.

The average Summer day scenario is the most interesting in this setting. Physically, this is because this MES is most interconnected in its ability to supply cooling demand from steam (boilers and CHP driving absorption chiller) and electricity (battery and CHP driving the electric chiller). That is, in this MES case study, for Summer scenarios, building flexibility on its own appears to offer an alternative to carbon pricing. This is because with a 100% renewable energy utility, electrification becomes beneficial to carbon reduction goals. This shift in electricity imports is shown in Fig. 8(Right) for the extreme $2000/ton-CO2 price scenario and achieves an 84% reduction in CO2 emissions with a 60% increase in energy costs.

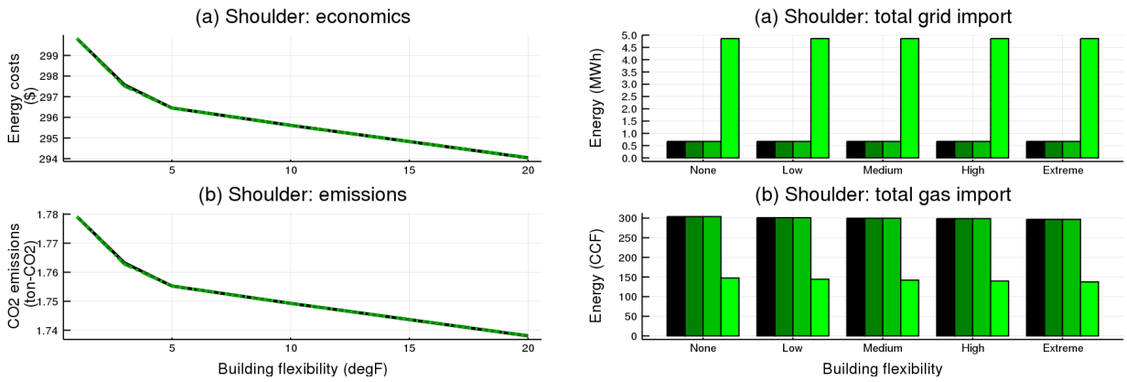

Figure 9: Simulation results for an average Shoulder season day for different levels of flexibility and carbon prices. *Left*: Energy costs and resulting emissions to understand (a) economics and (b) emissions. *Right*: energy imported from (a) grid and (b) gas pipeline suppliers to understand effects of flexibility and carbon prices.

4.1 Role of flexibility on economics and emissions

Increasing flexibility decreases overall economic energy costs under all carbon pricing scenarios. In the Winter and Shoulder seasons, the emissions decrease uniformly with increasing flexibility as well, which highlights the alignment between economic efficiency and reduced emissions for this MES – however, the effect of flexibility and carbon pricing is negligible in this MES. Thus, the focus of analysis is place on the Summer scenario. In the Summer case, the trade-off between CO2 and energy economics can lead to relative increases in emissions for increased flexibility, but overall positive CO2 pricing reduces emissions compared with having no price in place. Specifically, without a price on carbon, building flexibility in the Summer scenario alone is able to reduce economic costs by 3.5% and emissions by 7.4%. However, as we increase the price of CO2, we see expected increases in energy costs offset by decreases in CO2 emissions. This trade off in energy efficiency and CO2 emissions is expected from the objective function; however, as the level of building flexibility increases, the energy costs of a CO2 pricing policy can be greatly reduced by flexibility. Indeed, for \$100/ton-CO2 and \$150/ton-CO2 price scenarios, increased flexibility leads to relative cost reductions of up to 4.9% and 8.9%, respectively. This indicates that an MES operator should seek to strategically increase the coupling between heating, cooling, and electric demands in case of a carbon pricing and leverage building flexibility.

Table 11 shows the percentage reduction in CO2 from positive carbon pricing policies relative to the nominal flexibility-only case. That is, a value of 0% represents that for fixed flexibility value, θ_{Flex}, that the \$0/ton-CO2alone scenario can achieve the same CO2 reduction as with a carbon price. Clearly, flexibility significantly reduces the gap between having and not having a carbon price policy (or tax) in place. In fact, it is important to point out that (1) flexibility alone can significantly reduce CO2 emissions without a carbon tax and (2) with a carbon tax, flexibility can reduce the cost of implementing the policy. This is

an important outcome from this paper and shows that for a MES, like the one in Vermont, where electricity is already clean, thermal flexibility alone can have similar impact to a carbon tax. And this system is not particularly complex (i.e., limited options for dispatching assets), which highlights the need to further study (analytically and experimentally) this relationship between beneficial electrification, smart buildings (and thermal storage), and the impact of a carbon tax.

Table 11: Comparing carbon tax with no tax for Summer scenario (% CO2 reduction)

Flexibility	**1**	**3**	**5**	**10**	**20**
$0/ton-CO2	0	0	0	0	0
$100/ton-CO2	11.8	11.1	10.8	1.7	0.8
$150/ton-CO2	22.2	19.8	16.5	11.5	9.3

Table 12: Relative CO2 reductions (%)

	Flexibility	**1**	**3**	**5**	**10**	**20**
Winter	*$0/ton-CO2*	0	0.5	0.7	1.0	1.5
	$100/ton-CO2	0	0.5	0.7	1.0	1.5
	$150/ton-CO2	0	0.5	0.7	1.0	1.5
	$2000/ton-CO2	0	0.5	0.7	1.0	1.4
Summer	*$0/ton-CO2*	0	1.5	2.6	4.4	7.4
	$100/ton-CO2	0	0.9	1.8	-1.6	1.1
	$150/ton-CO2	0	-2.4	-7.1	-12.9	-11.7
	$2000/ton-CO2	0	0.4	0.1	4.2	11.5
Shoulder	*$0/ton-CO2*	0	0.9	1.3	1.7	2.3
	$100/ton-CO2	0	0.9	1.3	1.7	2.3
	$150/ton-CO2	0	0.9	1.3	1.7	2.3
	$2000/ton-CO2	0	2.2	3.7	5.2	6.8

Table 13: Relative costs reductions (%)

	Flexibility	**1**	**3**	**5**	**10**	**20**
Winter	*$0/ton-CO2*	0	0.4	0.4	0.7	1.0
	$100/ton-CO2	0	0.4	0.4	0.7	1.0
	$150/ton-CO2	0	0.4	0.4	0.7	1.0
	$2000/ton-CO2	0	0.1	0.1	0.7	0.2
Summer	*$0/ton-CO2*	0	0.7	1.2	2.1	3.5
	$100/ton-CO2	0	0.6	1.1	3.3	4.9
	$150/ton-CO2	0	1.5	4.0	7.2	8.9
	$2000/ton-CO2	0	1.9	4.8	6.6	8.3
Shoulder	*$0/ton-CO2*	0	0.7	1.1	1.4	1.9
	$100/ton-CO2	0	0.8	1.1	1.4	1.9
	$150/ton-CO2	0	0.8	1.1	1.4	1.9
	$2000/ton-CO2	0	0.5	0.9	1.3	1.7

Unlike Table 11, which compares the effect of carbon pricing on CO2 emissions, Tables 12 and 13 show the relative impact of increased flexibility in reducing CO2 emissions and energy costs for all four different carbon pricing policies. Interestingly, these results show that increased flexibility uniformly reduces economic costs (i.e., each row has increased reductions from left to right). This is because flexibility is used to co-optimize energy and carbon to minimize overall costs. More importantly, the results also indicate that flexibility alone (without carbon tax) reduces CO2 emissions for each carbon tax scenario (as illustrated in Figs. 7(Left)-9(Left)). Indeed, outside of the Summer scenario, we see that flexibility may be a useful mechanism to reduce both economic costs and emissions in a Vermont MES. For the summer, the flexibility is used to drive down costs by emitting $> 10\%$ extra CO2 to reduce energy costs by $> 7\%$ for the \$150 per ton-CO2 price scenario. The \$100/ton-CO2 case achieves a reduction in emissions and economics of 1.1% and 4.9%, respectively, from extreme (20°F) flexibility. Impressively, thermal flexibility in the Summer sees significant emission ($4-12\%$) and economic ($\approx 8\%$) gains in the case of extreme (\$2000) carbon pricing.

Thermal flexibility alters how the MES chooses to dispatch its assets. Next, we consider the optimized asset dispatch (i.e., actual optimal solution) for the specific scenario with

$0/ton-CO2 carbon price for a weekday's demand in each of the three seasons and for the two building flexibilities 1°F (None) and 20°F (Extreme). Figure 10 shows the ambient (exogenous input) and internal (optimized) temperature of the buildings in the Winter while Figs. 11 show the optimized electric and heating sources and conversions, including the flexible buildings' optimized heating building load. Note that the difference between electric demand and electric supply (i.e., CHP and grid imports) is made up by the battery, which charges when "Net battery" is negative and discharges when positive. Also, the CHP is allowed to vent steam, which is treated as a load as illustrated in Fig. 13a around hour 5.

Additional results are presented for Summer and Shoulder seasons in Figs. 12-15. Note that Summer includes another figure on cooling sources, which are used to pre-position energy in the building with the chillers output. The Shoulder season operates in a similar manner to Winter. The key to the economic and emission improvement gains in the Summer simulation with flexibility is from greatly improved efficiency. Notice that both heating and cooling in Fig. 13c and 13e operate during most of the day but on the lower end of their range (i.e., the low, inefficient 0.1-0.2 MMBtu/hr range of operations) when no flexibility is available. However, with flexibility, heating and cooling moves to sporading, but much more efficient operating points (i.e., the high, 0.5 MMBtu/hr range per device). While the sporadic dispatch incurs additional startup costs, they are much smaller than the efficiency gains.

Remark (Flexibility and ramping)**.** *The MILP formulation includes ramp-rate limits on energy converters to limit excessive ramping, which, in practice, reduces efficiency, increases wear and tear, and, thus, should be avoided. The ramp-rate limits were added (per plant operator's recommendations) to capture the effects of ramp-up limits and minimum start-up time for boilers, which is on the order of 15-30 minutes and necessary to build up pressure in the boiler's drum. Flexibility has interesting effects on the asset dispatch across the Winter, Summer, and Shoulder periods. Without flexibility the assets have to responds rapidly to changes in demand which increases ramping (and creates the spiky dispatch on the left side of figures). The optimizer uses building flexibility to stage the equipment to avoid sudden jumps and cycling.).*

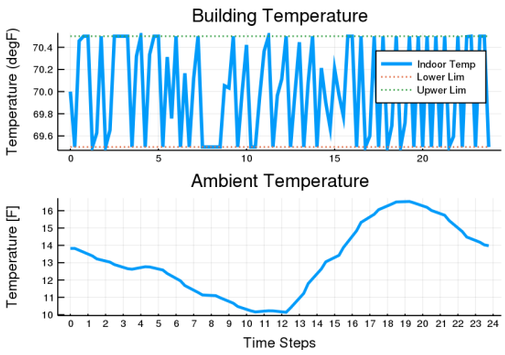

(a) No flexibility

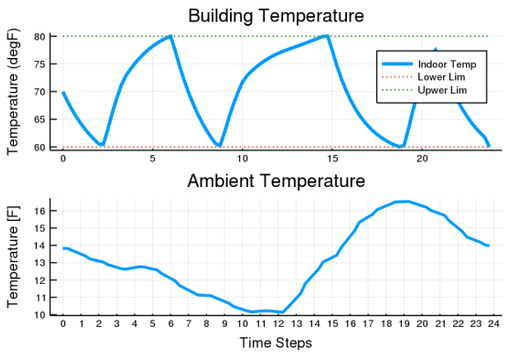

(b) Extreme flexibility

Figure 10: Winter indoor and ambient temperatures

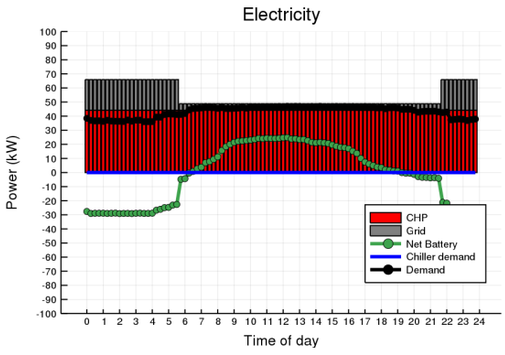

(a) Winter electric with no flexibility

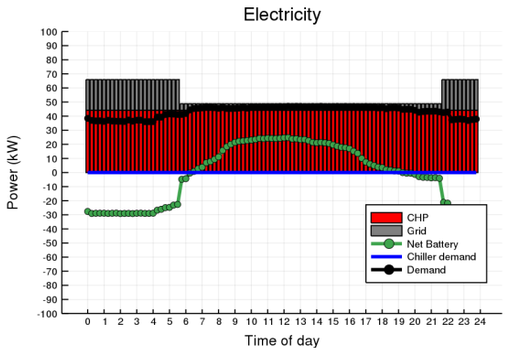

(b) Winter electric with high flexibility

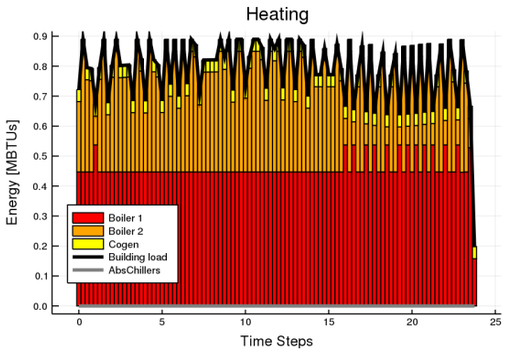

(c) Winter heating with no flexibility

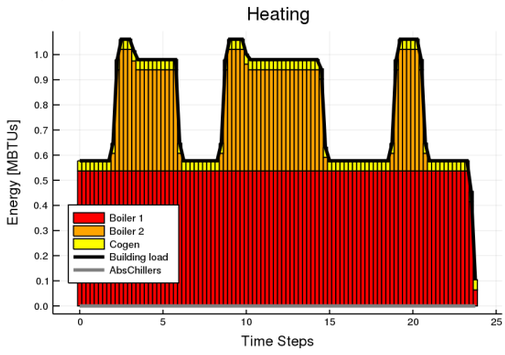

(d) Winter heating with extreme flexibility

Figure 11: Optimal dispatch for winter

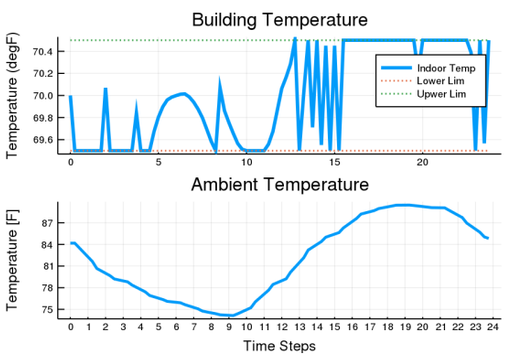

(a) No flexibility

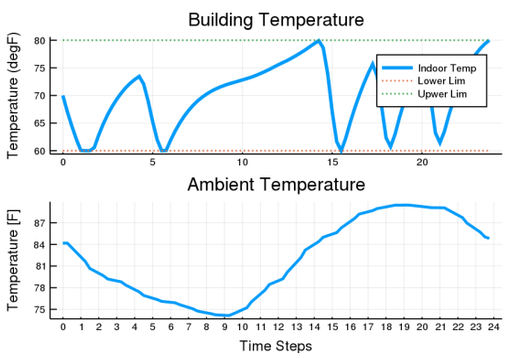

(b) Extreme flexibility

Figure 12: Summer indoor and ambient temperatures

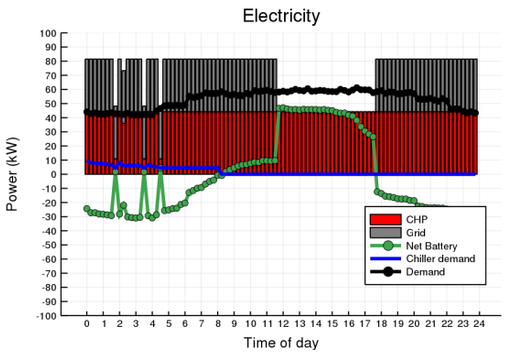

(a) Summer electric with no flexibility

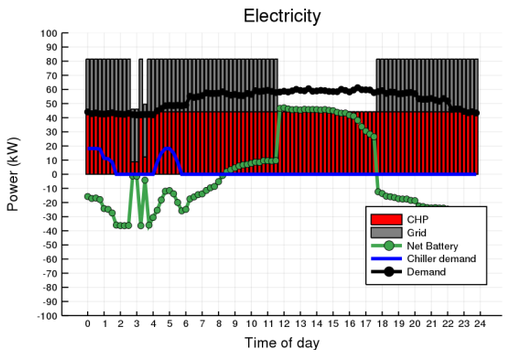

(b) Summer electric with extreme flexibility

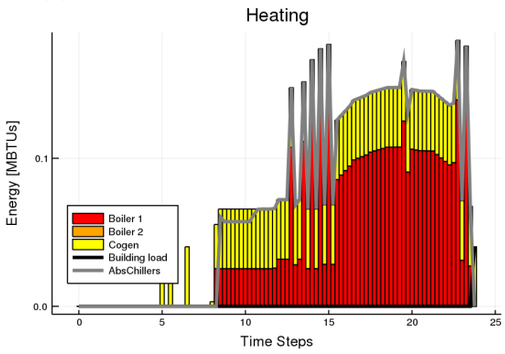

(c) Summer heating with no flexibility

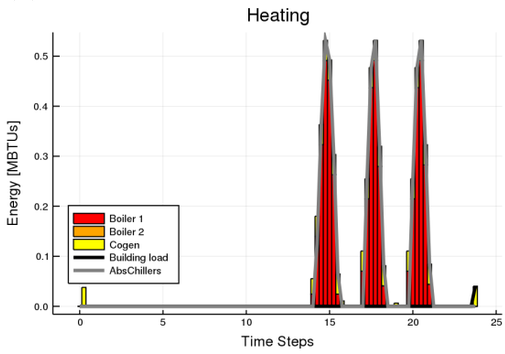

(d) Summer electric with extreme flexibility

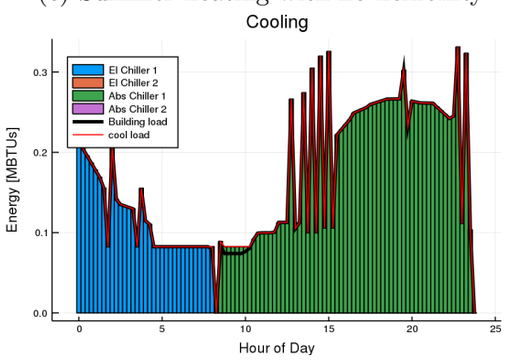

(e) Summer chillers with no flexibility

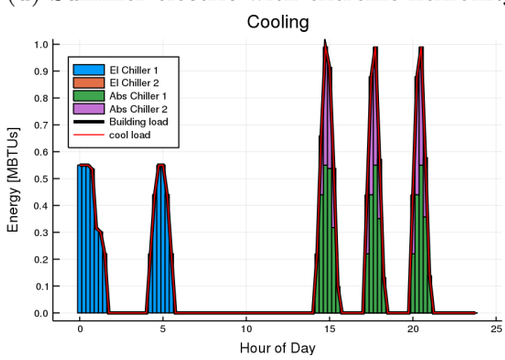

(f) Summer chillers with extreme flexibility

Figure 13: Optimal dispatch for Summer

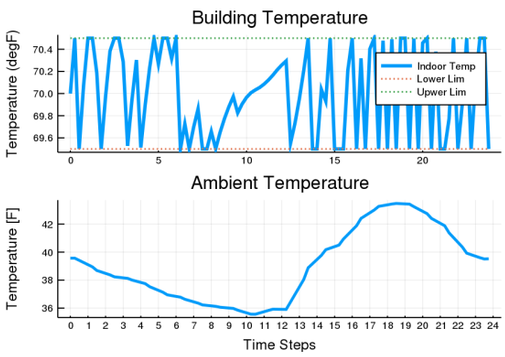

(a) No flexibility

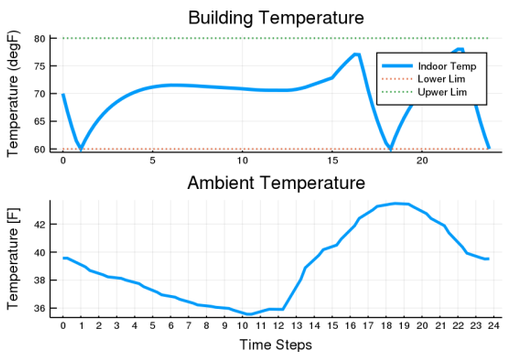

(b) Extreme flexibility

Figure 14: Shoulder indoor and ambient temperatures

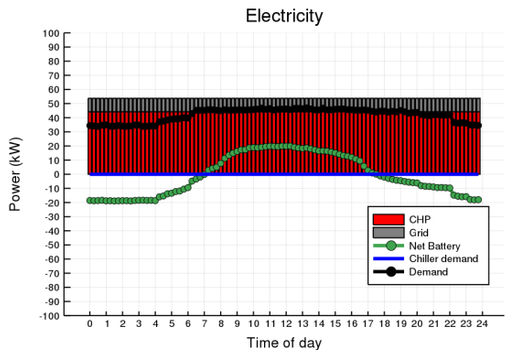

(a) Shoulder electric with no flexibility

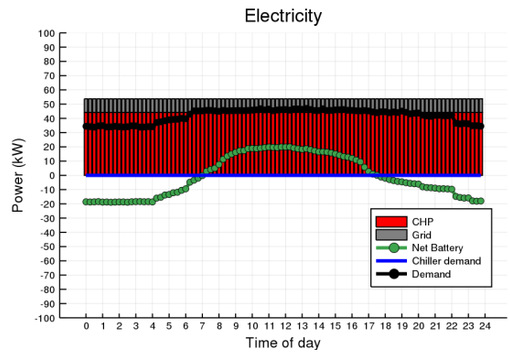

(b) Shoulder electric with extreme flexibility

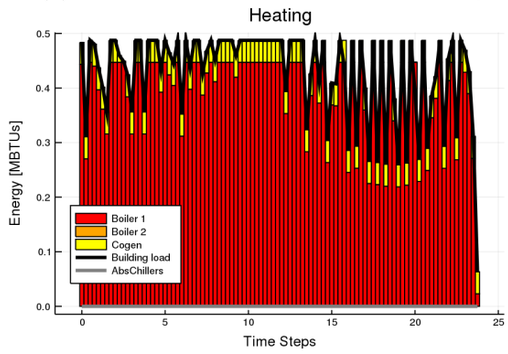

(c) Shoulder heating with no flexibility

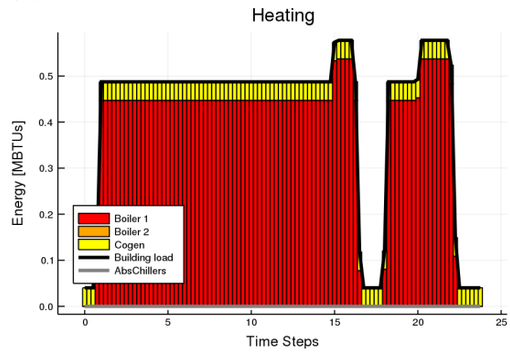

(d) Shoulder heating with extreme flexibility

Figure 15: Optimal dispatch for Shoulder

Finally, it is worth pointing out that the amount of energy saved is relative to the ambient temperature and the base amount of energy needed without flexibility. In winter, a 20 degree increase in building flexibility (extreme) sees an equivalent of almost 80,000 BTUs of thermal energy storage. While in the summer, 20 degrees of flexibility is the equivalent of reducing load by 8,000 BTUs throughout the day.

Unfortunately, the building flexibility does not affect the electric supply side in Winter and Shoulder seasons as evidenced by the identical dispatch of the CHP and battery and import from the grid in Figs. 11a and 11b and Figs. 15c and 15d. Due to the rate structure's high demand charges and, as evidenced in Figs. 7(Right)-9(Right), the CHP is dispatched for any realistic carbon price scenario. compared with natural gas, it will always be more cost effective to run the CHP and use the battery to reduced peak usage as much as possible independent of what happens on the cooling and heating side. The battery charges early in the day (as negative electric supply in Figs. 13a and 13a) to then use the stored energy during peak hours to cut the peak demand and usage from the grid, this is the largest cost saver and the strategy does not change with added flexibility. This dispatch pattern might tilt towards more flexible buildings and gas assets, if we changed BED's electric supply from 100% renewable to, say, 50% renewable and applied a carbon-tax, which could now increase the price of electricity substantially and make the electric battery too expensive to dispatch. A large-scale sensitivity study along with this model could aid policy-maker rank a number of policy-options by their effectiveness across the MES.

4.2 The need for policy and flexible building technology

Under a carbon tax, the operation strategy for the MES does not change significantly since the electric utility (i.e., electric supply) is 100% renewable.Further increasing the carbon tax would eventually cause the system to switch to focus on mitigating natural gas consumption. Increased flexibility means less cooling or heating is required thereby less resources are used and, more importantly, the resources are used more efficiently to ensure less fuel is used to supply demand. Furthermore adding more flexible buildings and electric heating to the system would give the MES tool more options over which to optimize and costs and emissions performance. However, adding more flexibility to the MES comes at the cost of convenience to occupants, so there is a need to develop technologies that anonymously and autonomously unlock flexibility without noticeably sacrificing comfort of the MES occupants. This puts the onus on design and operation of modern buildings, especially those that are energy conscious, to take full advantage of this intrinsic thermal storage to improve MES operations and efficiency, reduce emissions further, and manage costs.

5 Conclusion and future work

In this paper, we aimed to identify the effects of flexibility within a Vermont-based MES. The electric, heating, and cooling demand, as well as, thermal and physical parameters for the equivalent building model were derived using historical MES data while the internal, nonlinear energy processes that drive the results were modeled using PWL approximations to estimate asset input-output performance. This MES was then formulated as a 24-hour, day-ahead MILP planning problem with a resolution of 15-minute time-steps and tested seasonally for different flexibility and carbon tax scenarios. It was then shown that increased thermal flexibility not only reduces costs of operation but also can positively impact and reduce emissions. For this reason, flexibility may be more valuable in Vermont (and other high renewable electricity settings) than just a carbon tax, especially if the technology in place or the building design is constructed in a manner that can take the advantage of flexibility.

For future work, we seek to augment building data sets with time-series temperature data and perform high-fidelity building validation across different thermal building models and demonstrate the ability of flexibility to improve efficiency and study the effect on ramping and cycling of assets. In addition, this paper indicated that Winter and Spring are too "inflexible" in their MES capabilty and would benefit from electric-to-heat resources like heat-pumps and hot water storage [24] to increase it's ability to benefit from flexible buildings. We are also interested to study how uncertainties in predicted demand and building model parameters

affect the results and how a robust implementation may offer another avenue for directional recommendation that does not negatively affecting occupants. Finally, we would be excited to pursue testing with the physical plant division at the university to validate these results in a realistic setting to quantify the CO2 reductions and savings possible with flexible buildings.

Acknowledgements

We would like to thank Mr. Mike Pelletier of UVM Physical Plant Department for assistance and support in data gathering, model verification, and helpful discussions.

References

[1] Usman W. Chohan. "A Green New Deal: Discursive Review and Appraisal". In: *Notes on the 21st Century (CBRI)* (Mar. 2019).

[2] Joeri Rogelj et al. "Mitigation pathways compatible with 1.5C in the context of sustainable development". In: *Special Report on the impacts of global warming of 1.5 C*. Geneva: Intergovernmental Panel on Climate Change, 2018. URL: http://www.ipcc.ch/report/sr15/.

[3] et al. Ninoslav Holjevac. "Corrective receding horizon scheduling of flexible distributed multi-energy microgrids". In: *Applied Energy* 207 (Dec. 2017), pp. 176–194.

[4] Mads Almassalkhi et al. "Asynchronous Coordination of Distributed Energy Resources with Packetized Energy Management". In: *Energy Markets and Responsive Grids: Modeling, Control, and Optimization*. Ed. by Sean Meyn et al. New York, NY: Springer New York, 2018, pp. 333–361.

[5] He Hao et al. "Transactive Control of Commercial Buildings for Demand Response". In: *IEEE Transactions on Power Systems* 32 (Jan. 2016). DOI: 10.1109/TPWRS.2016.2559485.

[6] James B. Rawlings et al. "Economic MPC and Real-time Decision Making with Application to Large-Scale HVAC Energy Systems". In: *Computers & Chemical Engineering* 114 (Nov. 2017). DOI: 10.1016/j.compchemeng.2017.10.038.

[7] Jin X et al. "Dynamic Economic Dispatch of a Hybrid Energy Micro-Grid Considering Building Based Virtual Energy Storage System". In: *Applied energy* 194 (2017), pp. 386–398. ISSN: 0378-7788.

[8] Mads Almassalkhi, Bjorn Simon, and Archie Gupta. "A novel online energy management solution for energy plants". In: *IEEE Power Systems Conference*. Mar. 2014.

[9] M. J. Risbeck et al. In: *Hierarchical Microgrid Energy Management in an Office Building*. July 2015, pp. 1689–1694. DOI: 10.1109/ACC.2015.7170976.

[10] M.R.Almassalkhi and A.Towle. "Enabling City-scale Multi-energy Optimal Dispatch With Energy Hubs". In: *2016 Power Systems Computation Conference (PSCC)*. June 2016. DOI: 10.1109/PSCC.2016.7540981.

[11] *LEED V4 for Building Operations and Maintenance*. U.S. Green Building Council, 2018.

[12] Pierluigi Mancarella. "MES (multi-energy systems): An Overview of Concepts and Evaluation Models". In: *Energy* 65.c (Feb. 2014), pp. 1–17.

[13] B Bakken, HI Skjelbred, and Ove Wolfgang. "eTransport: Investment planning in energy supply systems with multiple energy carriers". In: *Energy* 32 (2007), pp. 1676–1689. DOI: 10.1016/j.energy.2007.01.003. URL: http://linkinghub.elsevier.com/retrieve/pii/S0360544207000175.

[14] Seungwon An, Qing Li, and Thomas Gedra. "Natural gas and electricity optimal power flow". In: *IEEE PES T&D Conference and Exhibition* 1 (2003), pp. 138–143.

[15] Martin Geidl and Göran Andersson. "A modeling and optimization approach for multiple energy carrier power flow". In: *In Proc. of IEEE PES PowerTech, St. Petersburg, Russian Federation* (2005), pp. 1–7. DOI: 10.1109/PTC.2005.4524640.

[16] K. Heussen et al. "Unified System-Level Modeling of Intermittent Renewable Energy Sources and Energy Storage for Power System Operation". In: *IEEE Systems Journal* 6.1 (Mar. 2012), pp. 140–151. ISSN: 1932-8184.

[17] Mads Almassalkhi and Ian A Hiskens. "Optimization Framework for the Analysis of Large-scale Networks of Energy Hubs". In: *Power Systems Computations Conference* (Aug. 2011).

[18] D. J. Olsen et al. "Planning Low-Carbon Campus Energy Hubs". In: *IEEE Transactions on Power Systems* 34.3 (May 2019), pp. 1895–1907.

[19] Enrico Fabrizio, Marco Filippi, and Joseph Virgone. "An hourly modelling framework for the assessment of energy sources exploitation and energy converters selection and sizing in buildings". In: *Energy and Buildings* 41.10 (Oct. 2009), pp. 1037–1050.

[20] Y. Ma, J. Matuško, and F. Borrelli. "Stochastic Model Predictive Control for Building HVAC Systems: Complexity and Conservatism". In: *IEEE Transactions on Control Systems Technology* 23.1 (Jan. 2015), pp. 101–116.

[21] Achin Jain et al. “Digital Twins for Efficient Modeling and Control of Buildings: An Integrated Solution with SCADA Systems”. In: *2018 Building Performance Analysis Conference and SimBuild*. Sept. 2018.

[22] Jin X et al. “Scheduling Distributed Energy Resources and Smart Buildings of a Microgrid via Multi-time Scale and Model Predictive Control Method”. In: *IET Renewable Power Generation* 13(6) (2018), pp. 816–833.

[23] Jiang T et al. “Flexible Operation of Active Distribution Network Using Integrated Smart Buildings with Heating, Ventilation and Air-conditioning Systems”. In: *Applied energy* 226 (2018), pp. 181–196.

[24] Ninoslav Holjevac, Tomislav Capuder, and Igor Kuzle. “Adaptive control for evaluation of”. In: *Energy* 92.Part 3 (Dec. 2015), pp. 487–504.

[25] Refrigerating American Society of Heating and Air-Conditioning Engineers. *The ASHRAE Handbook Fundamentals (I-P Edition)*. New York: The Society, 2005.

[26] *EPA’s Treatment of Biogenic Carbon Dioxide (CO2) Emissions from Stationary Sources that Use Forest Biomass for Energy Production*. Environmental Protection Agency, 2018.

[27] Christopher Recchia. *Vermont Comprehensive Energy Plan*. Vermont Department of Public Service, 2016.

[28] Z. Li et al. “Sufficient Conditions for Exact Relaxation of Complementarity Constraints for Storage-Concerned Economic Dispatch”. In: *IEEE Transactions on Power Systems* 31.2 (Mar. 2016), pp. 1653–1654.

[29] M. R. Almassalkhi and I. A. Hiskens. “Model-Predictive Cascade Mitigation in Electric Power Systems With Storage and Renewables—Part I: Theory and Implementation”. In: *IEEE Transactions on Power Systems* 30.1 (Jan. 2015), pp. 67–77.

[30] Abdul Ghafoor Memon and Rizwan Ahmed Memon. “Parametric Based Economic Analysis of a Trigeneration System Proposed for Residential Buildings”. In: *Sustainable Cities and Society* 34 (2017), pp. 144–158. ISSN: 2210-6707. DOI: https://doi.org/10.1016/j.scs.2017.06.017. URL: http://www.sciencedirect.com/science/article/pii/S2210670717301762.

[31] Yashen Lin, Timothy Middelkoop, and Prabir Barooah. “Issues in identification of control-oriented thermal models of zones in multi-zone buildings”. In: *Proceedings of the IEEE Conference on Decision and Control*. 2012, pp. 6932–6937.

[32] Wesley J. Cole et al. “Reduced-order Residential Home Modeling for Model Predictive Control”. In: *Energy and Buildings* 74 (2014), pp. 69–77. ISSN: 0378-7788. DOI: https://doi.org/10.1016/j.enbuild.2014.01.033. URL: http://www.sciencedirect.com/science/article/pii/S0378778814000711.

[33] Antoine Lesage-Landry et al. “Online Convex Optimization of Multi-Energy Building-to-Grid Ancillary Services”. In: *IEEE Transactions on Control Systems Technology (to appear)* (2019).

[34] M. Amini and M. Almassalkhi. “Trading Off Robustness and Performance in Receding Horizon Control with Uncertain Energy Resources”. In: *Power Systems Computation Conference (PSCC)*. June 2018.

[35] Mahraz Amini. “Optimal Dispatch of Uncertain Energy Resources”. PhD thesis. The University of Vermont and State Agricultural College, Burlington, Vermont, 2019.